



Article

Modeling Large River Basins and Flood Plains with Scarce Data: Development of the Large Basin Data Portal

Riham K. Abu-Saymeh 1,* , Adil Godrej 1 and Kathleen A. Alexander 2,3

- Department of Civil and Environmental Engineering, Virginia Tech, Blacksburg, VA 24061, USA
- Department of Fisheries and Wildlife Conservation, Virginia Tech, Blacksburg, VA 24061, USA; kathyalx@vt.edu
- ³ Centre for Conservation of African Resources: Animals, Communities and Land Use (CARACAL), Kasane, Botswana
- * Correspondence: riham99@vt.edu

Abstract: Hydrological modeling of large river basins and flood plains continues to be challenged by the low availability and quality of observed data for modeling input and model calibration. Global datasets are often used to bridge this gap, but are often difficult and time consuming to acquire, particularly in low resource regions of the world. Numerous calls have been made to standardize and share data to increase local basin modeling capacities and reduce redundancy in efforts, but barriers still exist. We discuss the challenges of hydrological modeling in data-scarce regions and describe a freely available online tool site developed to enable users to extract input data for any basin of any size. The site will allow users to visualize, map, interpolate, and reformat the data as needed for the intended application. We used our hydrological model of the Upper Zambezi basin and the Chobe-Zambezi floodplains to illustrate the use of this online toolset. Increasing access and dissemination of hydrological modeling data is a critical need, particularly among users where data requirements and access continue to impede locally driven management of hydrological systems.

Keywords: large river basins; hydrodynamic model; scarce data



Citation: Abu-Saymeh, R.K.;
Godrej, A.; Alexander, K.A. Modeling
Large River Basins and Flood Plains
with Scarce Data: Development of the
Large Basin Data Portal. Hydrology
2023, 10, 87. https://doi.org/
10.3390/hydrology10040087

Academic Editors: Samkele Tfwala, Chingnuo Chen and Su-Chin Chen

Received: 8 March 2023 Revised: 1 April 2023 Accepted: 4 April 2023 Published: 6 April 2023



Copyright: © 2023 by the authors. Licensee MDPI, Basel, Switzerland. This article is an open access article distributed under the terms and conditions of the Creative Commons Attribution (CC BY) license (https://creativecommons.org/licenses/by/4.0/).

1. Introduction

Large river basins such as the Amazon, Nile, and the Zambezi River Basins affect the livelihood of millions of people and the animals and landscapes on which they depend [1,2]. Changes in basin climate, the hydrodynamics of the connected river system, and changes in the human-built environment can profoundly impact basin hydrological dynamics and the people and ecosystems living in and around those areas [3,4]. Hydrodynamic modeling can provide a critical tool to evaluate and predict system function and the impact of potential changes, such as studying the impact of infrastructure development on water quality and hydropower potential [5,6].

Hydrological models have also been used extensively to predict potential flood extent and risk of agricultural damage [7–9]. These tools are also critical in predicting potential human health impacts, as flooding events may have considerable impacts on water quality and waterborne disease outbreaks in associated populations [10]. Predicting the start of a flooding event and flood water recession processes from upstream rainfall events may provide considerable lead time to prevent or mitigate expected impacts [11].

Modeling large river basins can also be used to improve water resource management and irrigation practices as water conditions change [12,13]. This can also be used to aid in resolving conflicts between various water authorities or countries sharing the use of river water by further understanding the problem, formalizing performance measures, and evaluating sharing scenarios and alternatives [14]. Models can also provide forecasts and insights into water availability for downstream nations [15].

Hydrology **2023**, 10, 87 2 of 22

The remotely derived data can serve as a robust proxy for incomplete or absent local data for large river basins, providing similar results to those obtained from the use of conventional local weather data. For example, remote sensed climate data from the National Centers for Environmental Prediction's Climate Forecast System Reanalysis (CFSR) were evaluated against local data sources and provided similar results for the hydrological characterization of the Upper Blue Nile Basin in Ethiopia [16]. Similarly, remote sensed data were used successfully to create a large-scale hydrodynamic model of the Amazon River Basin [17], outcomes that agreed with locally derived data sources.

The need for remote imagery is not limited to hydrological model development with remote sensing data used to evaluate historical basin flooding dynamics [18] and estimate flood extent [19–23]. These studies provide critical insight in the hydrological dynamics, but cannot be used to study future scenarios and forecast basin performance.

Not all data sourcing techniques rely on remote sensing options. For example, the recently developed soil erodibility factor calculation provides a mechanism to generate an estimate of sediment yield in watersheds based on sand, silt and clay percentages [24]. This tool can be used in data-scarce regions, with some studies providing less than a 20% error in the results [24].

Across all these applications, accurate and precise data are needed for effective modeling applications. Lack of data availability can have a negative impact on the accuracy of models [25,26] and other estimations, compromising the application and use of these models, particularly in resource limited regions of the world. Data scarcity can be particularly problematic for large basins that cover expansive regions [27–29], some with a total area of more than 1 million km² (e.g., the Zambezi River Basin covers eight countries in Africa with an area of 1.3 million km² [30]). These basins require macro-scale models [31] and a large amount of input data, which can be challenging to obtain [15]. Modeling river basins in western and more developed countries is often easier where climate, geographic and geological data are more widely available. Data scarcity continues to plague low resource environments where population vulnerability is elevated and the need for model access and improved forecasting capacity is escalating [32].

Here, we report the development of a freely available online data acquisition and manipulation resource, the Large Basin Data Portal, that can be used to support hydrological model development for any basin. A typical modeling effort incorporates five activities: (1) Input data source identification; (2) Input data extraction, remapping, and formatting; (3) Model development; (4) Model calibration using historical data; (5) Running the models and obtaining results. The Large Basin Data Portal simplifies the processes involved in modeling activities 1, 2, and 4. We provide a description of the methods used to create the site and provide an overview of site functionality and access. We also illustrate the use of the tools by modeling the Upper Zambezi River Basin and the Chobe–Zambezi flood plains, regions of the world with limited data. The Zambezi River is Africa's longest river, and the largest flowing into the Indian Ocean from Africa [33,34].

2. Materials and Methods

The Large Basin Data Portal was developed using a combination of HTML (Hyper-Text Markup Language), CSS (Cascaded Styling Sheets), and JavaScript for the user interface development, and PHP [35] scripts and C language modules [36] for the backend programming used to retrieve and process datasets. The portal incorporates several user tools than can be categorized into 3 categories: Data Extraction, Data Visualization, and Utility tools. The data processing flow for all the tools can be generalized into 6 stages (Figure 1). Section 2.1 describes these stages and the general methods used by these stages, while Section 2.2 describes the specific methods and datasets used by each tool.

Hydrology **2023**, 10, 87 3 of 22

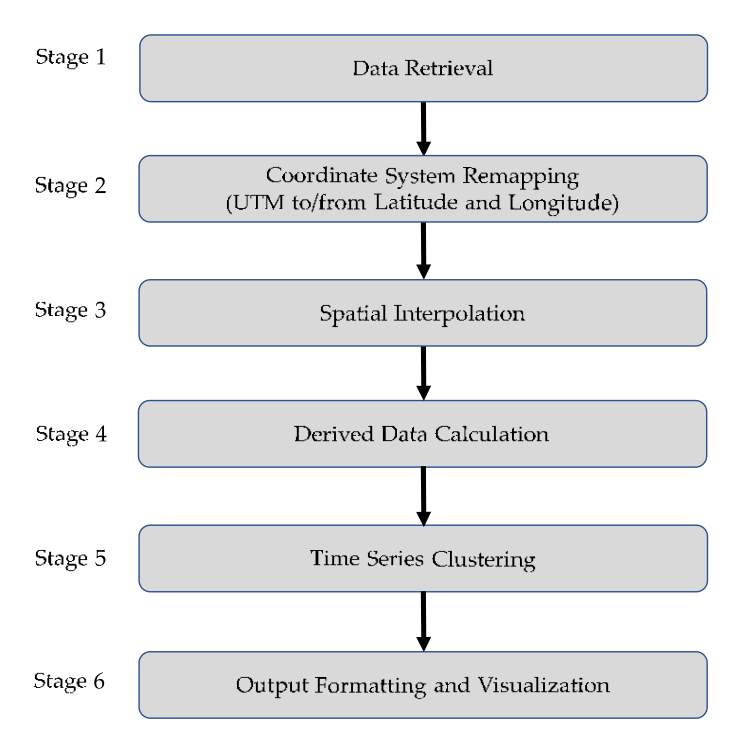


Figure 1. Data processing flow showing the 6 stages of data manipulation, starting with data retrieval from dataset source to final data output generation and visualization.

2.1. Data Processing Stages

2.1.1. Stage 1—Data Retrieval

Stage 1 of the data processing flow utilized Application Programming Interfaces (API) wherever available from the data providers. APIs allow granular data selection, which reduces the amount of data retrieved from the source to obtain the specific geographical area and time period required by the user. When APIs are not available for a data source, the data portal utilizes automatic dataset file download. In some cases, datasets are static and do not change, and these datasets are downloaded and maintained on the data portal. Table 1 shows the lists of data sources and datasets utilized by the tools available in the data portal and their data retrieval methods.

Table 1. Data sources and data sets used by the Large Basin Data Portal and their respective spatial and temporal resolution, spatial and temporal coverage, and retrieval methods.

Data Source Data Sets		Spatial and Temporal Resolution and Coverage	Data Retrieval Method	
	MOD09A1 (Terra Surface Reflectance)	500 m (Worldwide) 8-Day (2002–Present)	Location and time specific data retrieved automatically through the MODIS API when needed.	
Moderate Resolution Imaging Spectroradiometer (MODIS)	MCD12Q1 (Land Cover Type)	500 m (Worldwide) Annual (2001–Present)		
	MOD15A2H (Terra Leaf Area Index)	500 m (Worldwide) 8-Day (2002–Present)		
Google	Elevations	3 arc s (Worldwide)	Location specific data retrieved through online API as needed.	
Earth System Research	CPC Global Precipitation	0.5 (Worldwide) Daily (1979–Present)	Yearly global online dataset files	
Laboratory (ESRL) — Climate Prediction Center (CPC)	CPC Global Temperatures	0.5 (Worldwide) Daily (1979–Present)	- are downloaded automatically when needed.	
UN Food and Agriculture Organization (FAO)	Harmonized World Soil Database (HWSD)	30 arc s (Worldwide)	Static dataset files have been pre-downloaded into the data portal.	

Hydrology **2023**, 10, 87 4 of 22

2.1.2. Stage 2—Coordinate System Remapping

Stage 2 of the data processing flow maps the data coordinates between the UTM (Universal Transverse Mercator) and Longitude/Latitude coordinate systems as needed based on the model setup and the modeling tool used by modelers. UTM rectangular grids are widely used in modeling since they attempt to represent the modeled area as a flat surface in contrast to the spherical Latitude/Longitude system. The data portal uses the standard coordinate conversion calculations documented by the UTM geocoding standard [37].

2.1.3. Stage 3—Linear Spatial Interpolation

The diversity of the data sources generally results in data that do not have either the same temporal or spatial resolution. Transformation techniques need to be used to transform such data to a uniform modeling grid where all input data can be defined at each grid point.

Linear spatial interpolation is used when data availability is not at the exact grid points. Such cases include elevation and cases where data are defined in a different geo-reference system. In many cases, data are defined at specific latitude and longitude coordinates (spherical grid) while a modeling grid is in the Universal Transverse Mercator (rectangular grid). Linear spatial interpolation is performed in Stage 3 to generate data values at the desired grid points. Spatial interpolation is needed when converting data between coordinate systems and when upscaling or downscaling (sampling) to achieve the desired spatial data resolution.

The data value at any given point (not defined by the original data) can be derived from the surrounding 4 data points (corners of the rectangle that includes the desired point). Two types of spatial interpolation may be performed based on the data type. Qualitative data such as soil type use the data value at the nearest defined point (corners of the enclosing rectangle) based on distance. Quantitative data such as elevation, rainfall or temperature use the inverse distance weighting (IDW) methodology [38] based on the data values at the 4 enclosing rectangle corner points. The value u_k at any point k inside the enclosing rectangle can be calculated using:

$$u_{k} = \frac{\mathring{a}_{i=1}^{4} \frac{u_{i}}{u_{k,i}}}{\mathring{a}_{i=1}^{4} \frac{1}{d_{k,i}}}$$
(1)

where u_i is the value at point/corner i and $d_{k,i}$ is the distance between point k and point i.

2.1.4. Stage 4—Derived Data Calculation

Stage 4 of the data processing flow consists of several submodules that manipulate the data to derive new measurements (e.g., calculating reference evapotranspiration for daily temperatures). These submodules are specific to the measurements being derived, and are described in more detail when the tool that uses them is presented.

2.1.5. Stage 5—Time Series Clustering

Time-varying data with high spatial resolution such as LAI (Leaf Area Index) and land cover data generate very large amounts of input data that can considerably slow down model execution. Some modeling tools allows modelers to divide the modeled grid into groups of cells with a single time-series data file representing the input for that group of cells [39].

Stage 5 utilizes the K-Means data clustering algorithm [40] to group grid points into groups of points that have similar time-based profiles, thus reducing the number of time series profiles that need to be fed into models. The algorithm starts by grouping adjacent grid cells into a specific number of clusters N selected by the user. Higher N values will give more accurate results, but will produce a larger amount of data. Then, the average daily data value (e.g., daily LAI) is calculated for each cluster, generating a daily time-

Hydrology **2023**, 10, 87 5 of 22

series profile for each cluster. The statistical distance $d_{i,k}$ for each cell i to cluster k is then calculated as:

$$d_{i,k} = v_{i,j} p_{k,j}$$
all days j

where $v_{i,j}$ is the data value of cell i on day j and $p_{k,j}$ is the data value of cluster k profile on day j. Each cell is then reassigned to a cluster with the minimal statistical distance and the average daily profile for each cluster is recalculated. This reiterative approach is continued until cells are no longer reassigned to new clusters, or for a certain number of iterations.

2.1.6. Stage 6—Output Data Formatting

Stage 6 formats the data and creates files that can be utilized by the modeling software. In some cases, the data can be visualized on online maps which not only helps modelers, but is also useful for quick visual analysis of historical climatic events.

2.2. Output Data Validation

The outputs of the tools were validated using a manual comparison of the outputs with the original data from the source datasets. Tool output data were also compared to other datasets. The comparison was performed mainly for the Upper Zambezi River Basin, and the Occoquan watershed in northern Virginia, USA. The output of the flood mapper was also visually compared to historical satellite flood images available from NASA satellites [41].

2.3. Large Basin Data Portal—Data Extraction Tools

2.3.1. Elevation Grid Extraction

Elevation/Topology grids are the most critical input to any hydrological model. The topology of the modeled area governs how and where overland and underground water flows, creating streams and rivers and lakes. Within the Large Basin Data Portal, a user can easily obtain the required elevation grid for the area of interest by simply specifying the model's rectangular area and the resolution of the grid. The elevation data are then extracted from Google Maps [42] using an API in the background. The tool (Figure 2) then utilizes the Coordinate System remapping and Spatial interpolation stages to produce the final grid in the desired resolution. Finally, the grid is written to a CSV (Comma Separated Values) text file which can be used in or imported into various modeling programs. A simple demonstration of the use of the Elevation Grid Extraction tool and other data extraction tools is available in Video S1.

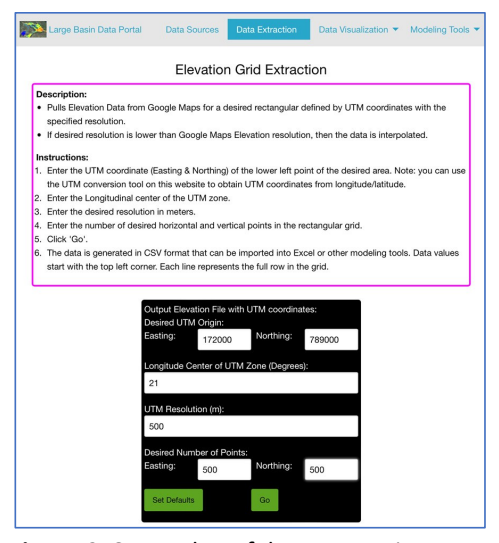


Figure 2. Screenshot of the Large Basin Data Portal elevation extraction tool with description, usage instructions, and input parameters.

Hydrology **2023**, 10, 87 6 of 22

2.3.2. Soil Type Extraction

Soil type represents the upper part of the unsaturated zone and is used to model surface water penetration into the ground. The soil type extraction tool (Figure 3) can be used to extract the soil type grid from the FAO HWSD global dataset [43], which combines regional and national databases of soil types and maps. The dataset has a spatial resolution of (0.00833). The spatial resolution is equivalent to 1 km near the equator. Since the desired grid points and the FAO HWSD grid points may not match, the tool uses data from the closest FAO HWSD grid point for each desired grid point.

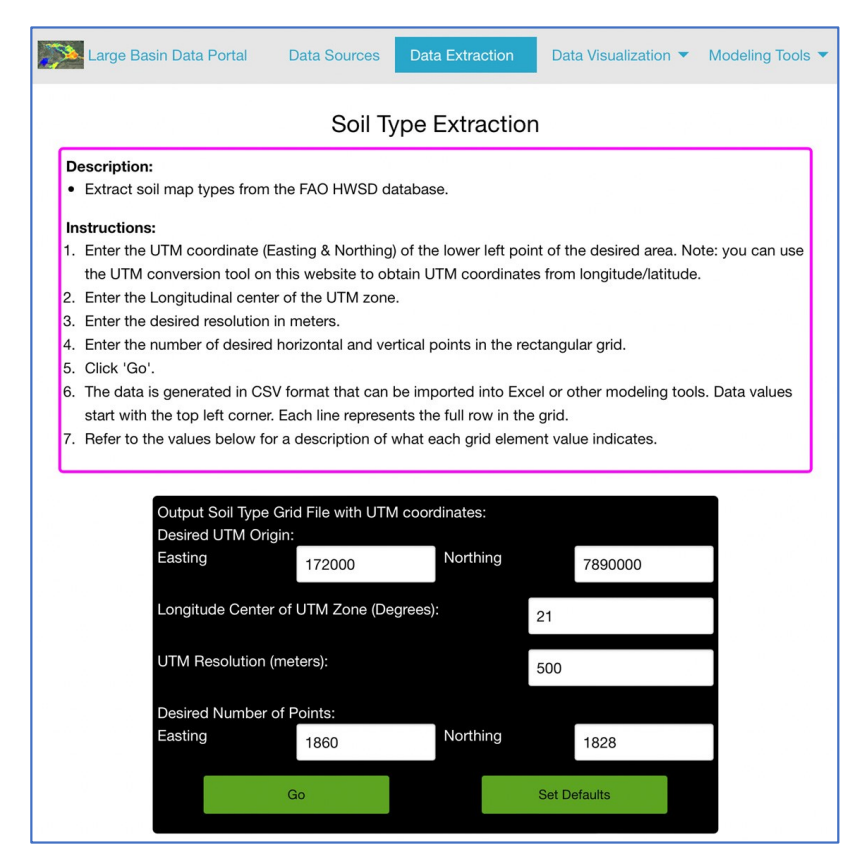


Figure 3. Screenshot of the Large Basin Data Portal soil type extraction tool with description, usage instructions, and input parameters.

2.3.3. Rainfall Extraction

The rainfall extraction tool (Figure 4) can be used to extract rainfall data from the NOAA ESRL CPC global rainfall dataset [44]. The ESRL data are derived from various remote sensors and have a spatial resolution of 0.5 (equivalent to 55 km near the equator) and a 1-day temporal resolution. The tool assigns each desired grid point to a cell group, and a time series of rainfall is produced for each cell group based on the desired time period. The user needs to specify the model's rectangular area and the resolution of the grid.

Hydrology **2023**, 10, 87 7 of 22

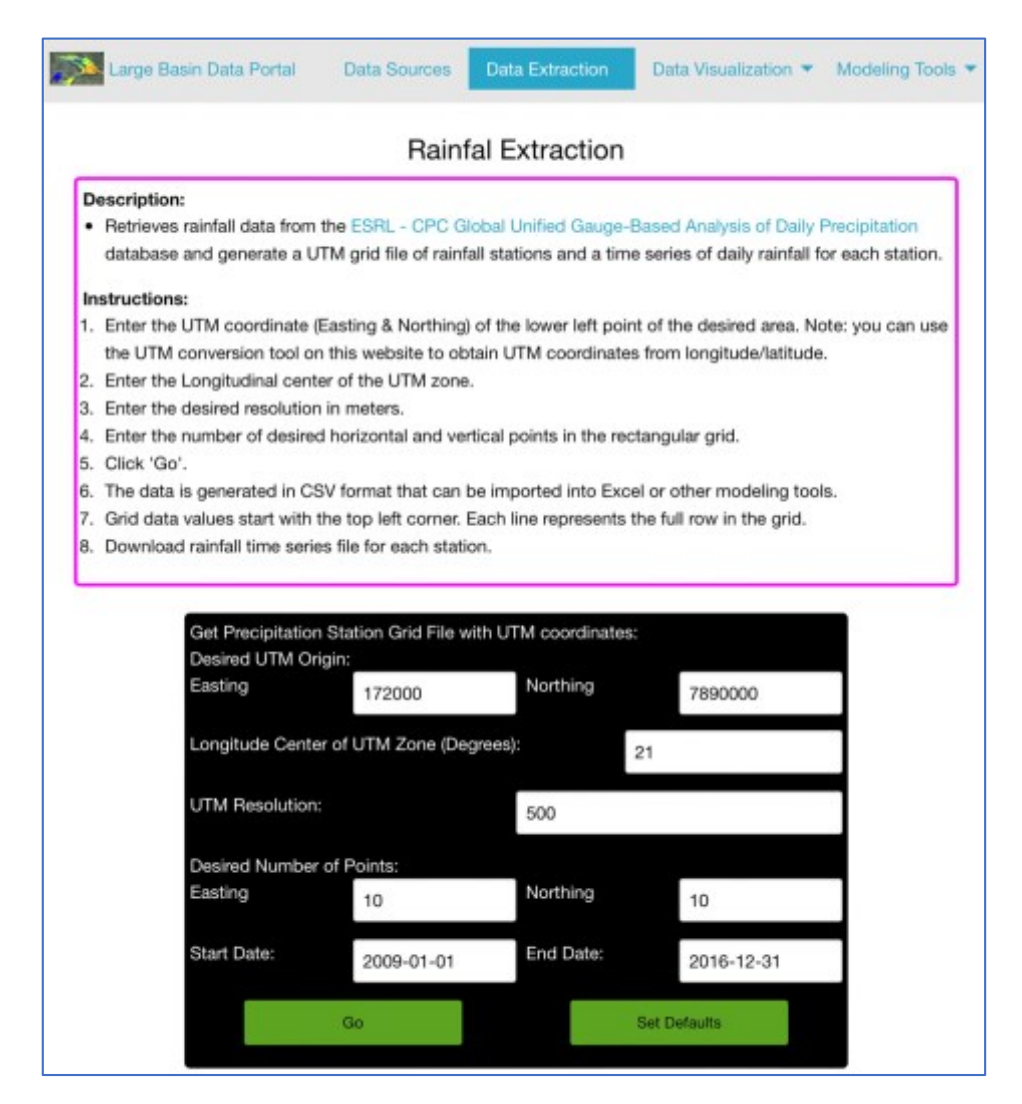


Figure 4. Screenshot of the Large Basin Data Portal rainfall extraction tool with description, usage instructions, and input parameters.

2.3.4. Leaf Area Index (LAI) Data Extraction

Many water modeling efforts, especially models that involve flooding, require LAI data to properly account for evapotranspiration. The LAI data extraction tool (Figure 5) gathers LAI data from NASA's MODIS MOD15A2H dataset [45]. MODIS datasets are derived from reflectance measurements at various wavelengths performed by the MODIS Terra and Aqua spacecraft. The dataset has a 500 m spatial resolution and an 8-day temporal resolution. For a large basin, the amount of data could be extremely large, so the tool uses the k-means clustering algorithm [40] to group grid points into areas of similar temporal LAI profiles (points that have similar LAI during the whole yearly cycle). The tool produces two separate outputs; the first is a grid with the assignment of each grid point to a specific LAI profile. The second is a time series of LAI data for each LAI profile. LAI data in this format are required by some modeling software [39].

Hydrology **2023**, 10, 87 8 of 22

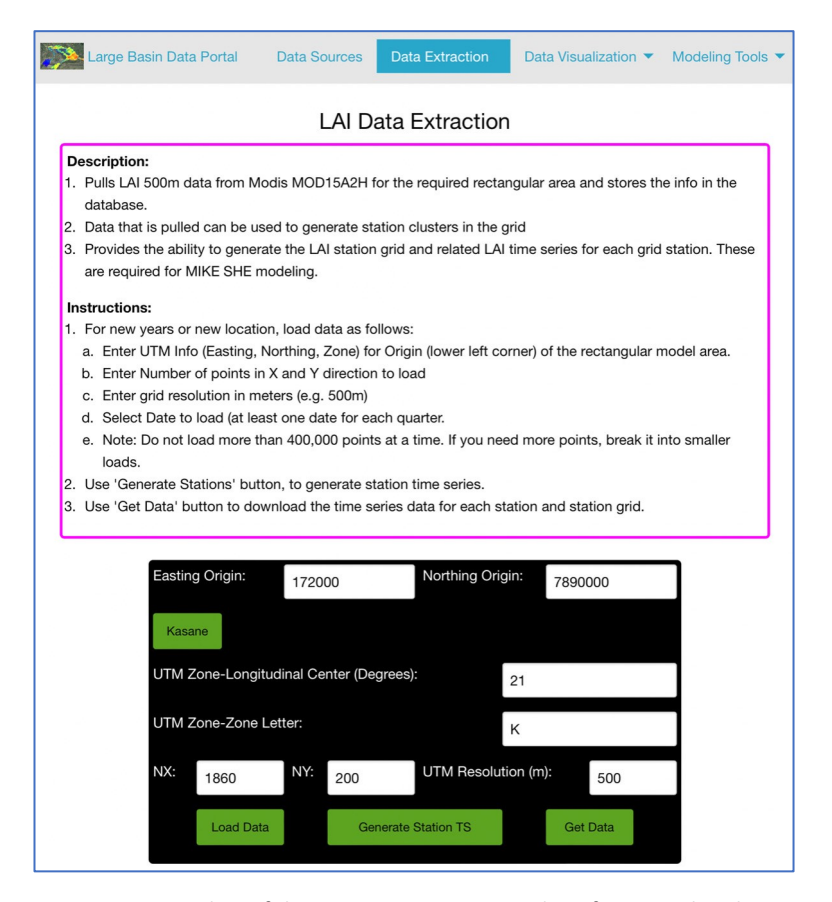


Figure 5. Screenshot of the Large Basin Data Portal Leaf Area Index data extraction tool with description, usage instructions, and input parameters.

2.3.5. Reference Evapotranspiration Data Extraction

Crop evapotranspiration is one of the critical pieces for modeling a water basin. Modeling software calculates the crop evapotranspiration based on a crop coefficient and reference evapotranspiration, which represents climate and solar conditions for the modeled area.

Reference evapotranspiration (ET_0) can be calculated using the Penman–Monteith equation [46] and standard climate input data. For large basins, not all climatic measurements are available for this equation, so the simplified version of the Penman–Monteith equation known as the Hargreaves equation [47] is used, which is based on daily max/min temperatures (T_{max} and T_{min}) as follows:

$$ET_0 = 0.0023R_a((T_{max} + T_{min})/2 + 17.8)^p \frac{1}{T_{max}} T_{min}$$
 (3)

where R_a is the surface radiation

$$R_a = \frac{2460}{p} G_{sc} d_r [w_s \sin j \sin d + \cos j \cos d \sin w_s]$$
 (4)

and G_{sc} is the solar constant (0.082 MJ/m²/day), d_r is the inverse relative distance of earth and sun, w_s is the sunset hour angle, and d is the solar decimation calculated using the Julian day of the year J and geographical latitude j of the location, as follows:

$$d_r = 1 + 0.003\cos \frac{2p}{365} J \tag{5}$$

$$w_{s} = \underbrace{p}_{tan} tan \underbrace{p}_{tan}$$
(6)

Hydrology **2023**, 10, 87 9 of 22

$$d = 0.409 \sin \frac{2p}{365} J \quad 1.39 \tag{7}$$

$$X = \max 1 (\tan i)^2 (\tan d)^2, 0.00001$$
 (8)

The reference evapotranspiration extract tool (Figure 6) downloads the daily min/max temperatures from ESRL's CPC Global temperature datasets [44]. The coordinates are then remapped from Longitude/Latitude to UTM. Spatial interpolation is then performed to obtain temperatures at the desired grid points, and the reference evapotranspiration is calculated. Finally, the results are written into CSV text files that can be used in various modeling programs.

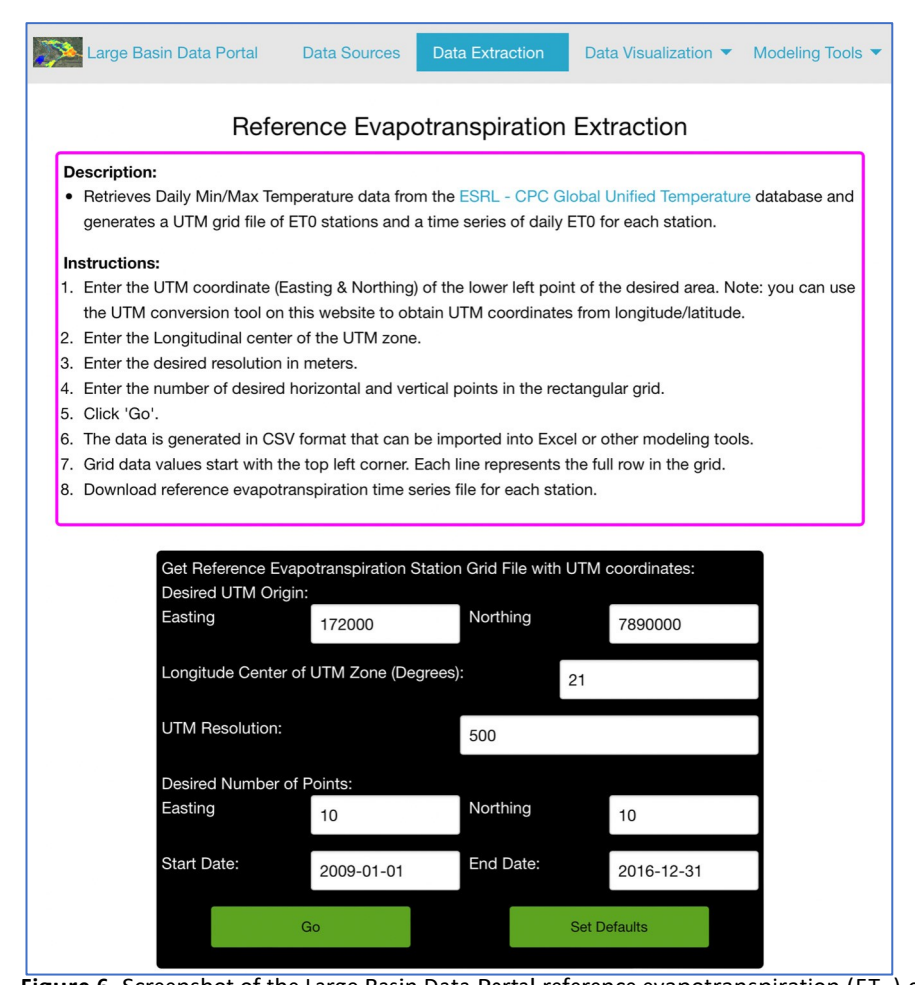


Figure 6. Screenshot of the Large Basin Data Portal reference evapotranspiration (ET_0) calculator with description, usage instructions, and input parameters.

2.4. Large Basin Data Portal—Data Visualization Tools

2.4.1. Flood Mapper

The Flood Mapper (Figure 7) extracts surface reflection data for various bands from the MODIS MOD09A1 dataset [48] and uses the algorithm described in [49] to derive the presence of overland water due to flooding events from reflectance measurements at various wavelength bands. The algorithm calculates NDWI (Normalized Difference Water Index) and NDVI (Normalized Difference Vegetation Index) as:

$$NDVI = (R_2 R_1)/(R_2 + R_1)$$
 (9)

Hydrology **2023**, 10, 87 10 of 22

$$NDWI = (R_2 R_6)/(R_2 + R_6)$$
 (10)

where R_1 is the reflectance in the wavelength range 620–670 nm, R_2 is reflectance in the wavelength range 841–876 nm, and R_3 is reflectance in the wavelength range 1628–1652 nm. Finally, the combination of NDVI, NDWI and the reflectance measurements are used to detect the presence of surface water at each grid cell, based on Table 2.

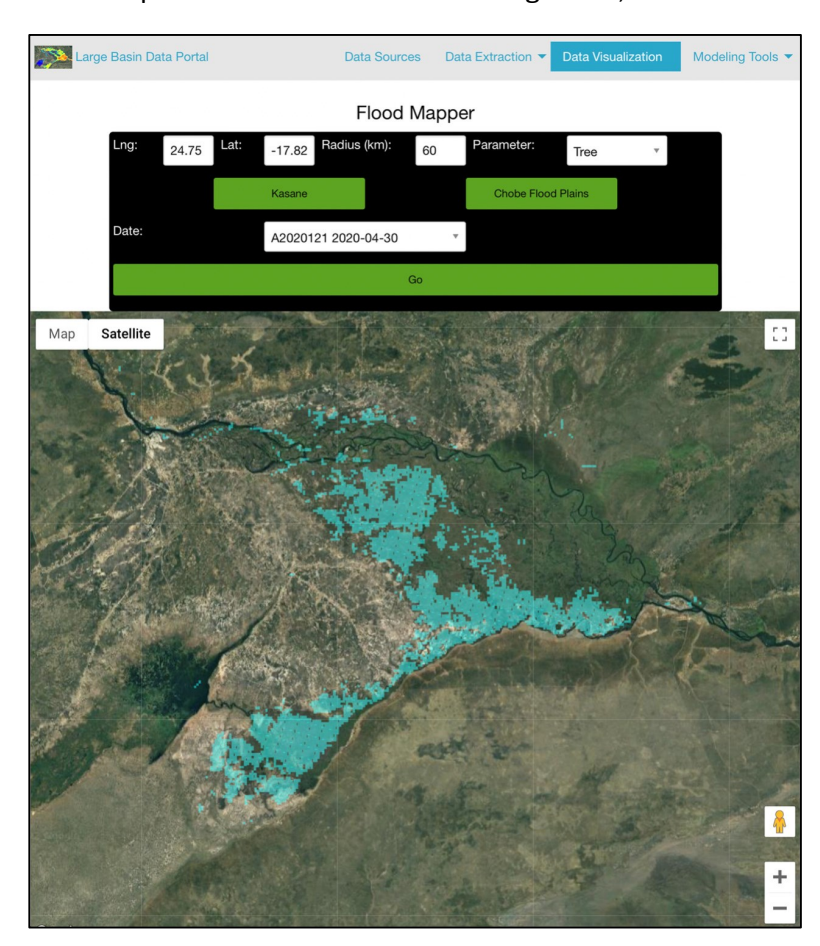


Figure 7. Screenshot of the Large Basin Data Portal flood mapper with input parameters and the displayed map of the Chobe–Zambezi floodplains, Africa. The blue overlay reflects the presence of surface water on 30 April 2020. The data are derived from MODIS MOD09A1 surface reflectance datasets.

Table 2. Criteria to classify whether surface water is present in each grid cell based on reflectance, Normalized Difference Vegetation Index, and Normalized Difference Water Index derived from MODIS datasets.

R ₁	R ₂	R ₂ -R ₁	NDVI	NDWI	Classification	
		>9.17			No Surface Water	
	>6.45		>0.5335		No Surface Water	
		>2.91	>0.228	0.2872	No Surface Water	
1.02		2.91			Water	
		2.91	<0.1509		Water	
		2.91		> 0.2931	Water	

The resulting water presence classification for each grid cell is then displayed on a Google map. The data have a 500 m spatial resolution and an 8-day temporal resolution and are available globally starting with the year 2000. A simple demonstration of the use of the Flood Mapper and other data visualization tools is available in Video S2.

Hydrology **2023**, 10, 87 11 of 22

2.4.2. LAI Mapper

To understand rainfall runoff into rivers and overland flood dynamics, it is helpful to visualize LAI for the modeled area, which has a significant impact on evapotranspiration. The LAI Mapper (Figure 8) retrieves LAI data from NASA's MODIS MOD15A2H dataset [45] using the MODIS API for the desired area, and displays them on a Google map.

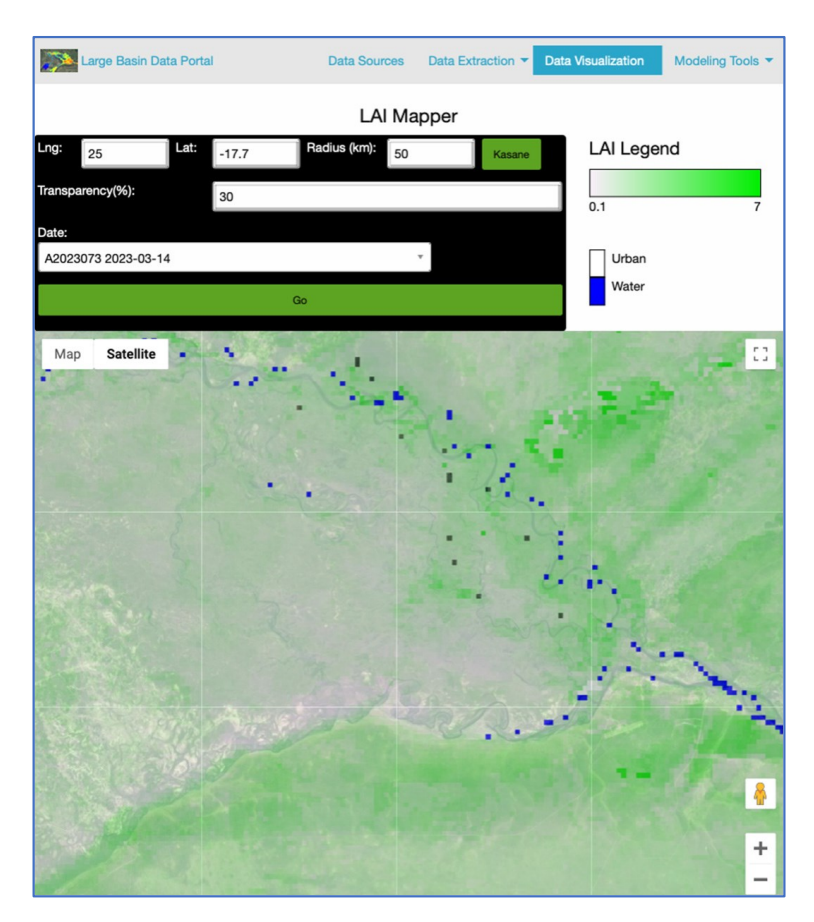


Figure 8. Screenshot of the Large Basin Data Portal Leaf Area Index (LAI) mapper with input parameters and the displayed map of the eastern section of the Chobe–Zambezi flood plains, Africa. The green shading overlay reflects various levels of LAI on 14 March 2023, based on data derived from the MODIS MOD15A2H dataset. The darker green areas represent areas with higher LAI (areas with higher plant/tree density).

2.4.3. Land Cover Mapper

Land Cover data are helpful in the overland modeling situation to determine overland water movement friction. A modeler can use the data to choose the correct Manning number for a 2D hydrodynamic model. For instance, forest areas would have a higher manning number than savannah lands. The Land Cover Mapper (Figure 9) retrieves Land Cover data from NASA's MCD12Q1 MODIS dataset [50] using the MODIS API, and displays the results on a Google map. The tool allows users to select one of 5 classification methodologies imbedded in the MCD12Q1 dataset: (1) Annual International Geosphere-Biosphere Programme (IGBP); (2) Annual University of Maryland (UMD); (3) Annual Leaf Area Index (LAI); (4) Annual BIOME-Biogeochemical (BGC); and (5) Annual Plant Functional Types (PFT).

Hydrology **2023**, 10, 87 12 of 22

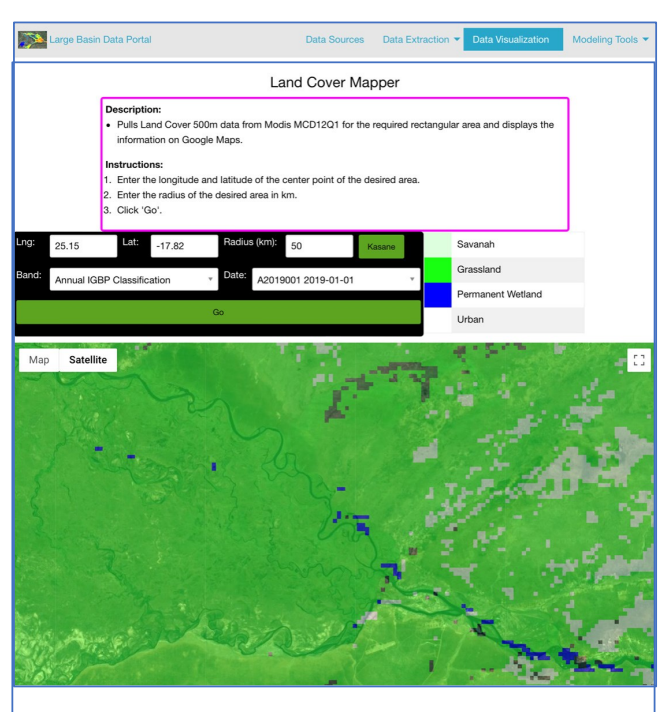


Figure 9. Screenshot of the Large Basin Data Portal land cover mapper with input parameters and the displayed map of the eastern section of the Chobe–Zambezi flood plains, Africa. The colored overlay represents different types of land cover type. Data are derived from the MODIS MCD12Q1 dataset for the year 2019, and are based on the Annual IGBP classification imbedded in the dataset.

2.5. Large Basin Data Portal—Other Modeling Tools

2.5.1. Lake and Land Depression Water Storage Capacity Calculator

Some river water basins contain natural storage lakes that store seasonal water. The amount of water stored depends on the topology of the surrounding area. As water levels increase, the water expands into larger areas that have an elevation lower than the water surface levels. In many locations, the volume of water that can be stored is unknown and may be needed for proper basin hydrology modeling.

The storage capacity of a land depression or a lake can be calculated using volume calculation methods of irregular conic frustums [51]. Given the elevation grid for an area, the minimum and maximum elevations of the grid are first calculated. Then, starting with the minimum elevation, contour lines are constructed for each elevation E_i in the grid with increments of 1 m (Figure 10).

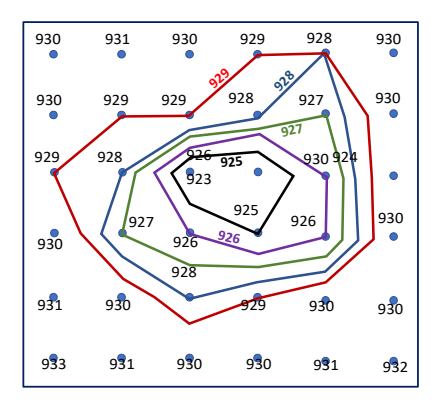


Figure 10. Illustration of elevation contour line construction for a sample elevation grid. The sample grid is a 6–6 grid with elevation at each grid point ranging from 923 m to 933 m above sea levels. In this example, contour lines for elevations 925 m, 926 m, 927 m, 928 m, and 929 m above sea level are constructed.

Hydrology **2023**, 10, 87 13 of 22

The area A_i within each contour line is then calculated to represent the surface area of the lake when the water surface level reaches elevation E_i . Finally, the lake potential water storage if water surface elevation reaches elevation E can be calculated as:

$$V_{E} = \frac{1}{3} \sum_{i=E_{min}}^{E} A_{i} + A_{i-1} + p_{A_{i} A_{i-1}}$$
 (11)

where E_{min} is the minimum surface elevation of the lake (surface elevation of the lake bottom), and A_i is the area of the lake within the contour line representing elevation E_i and A_{i-1} is the area of the lake within the contour line representing the next lower elevation E_{i-1} .

With the Lake/Land depression water storage capacity calculator (Figure 11), users enter the approximate geographical center of the lake and the search radius. The tool then downloads elevation data for the selected area from Google Maps using the API. The contour lines are then constructed and the area of each contour line and total storage volume is calculated.

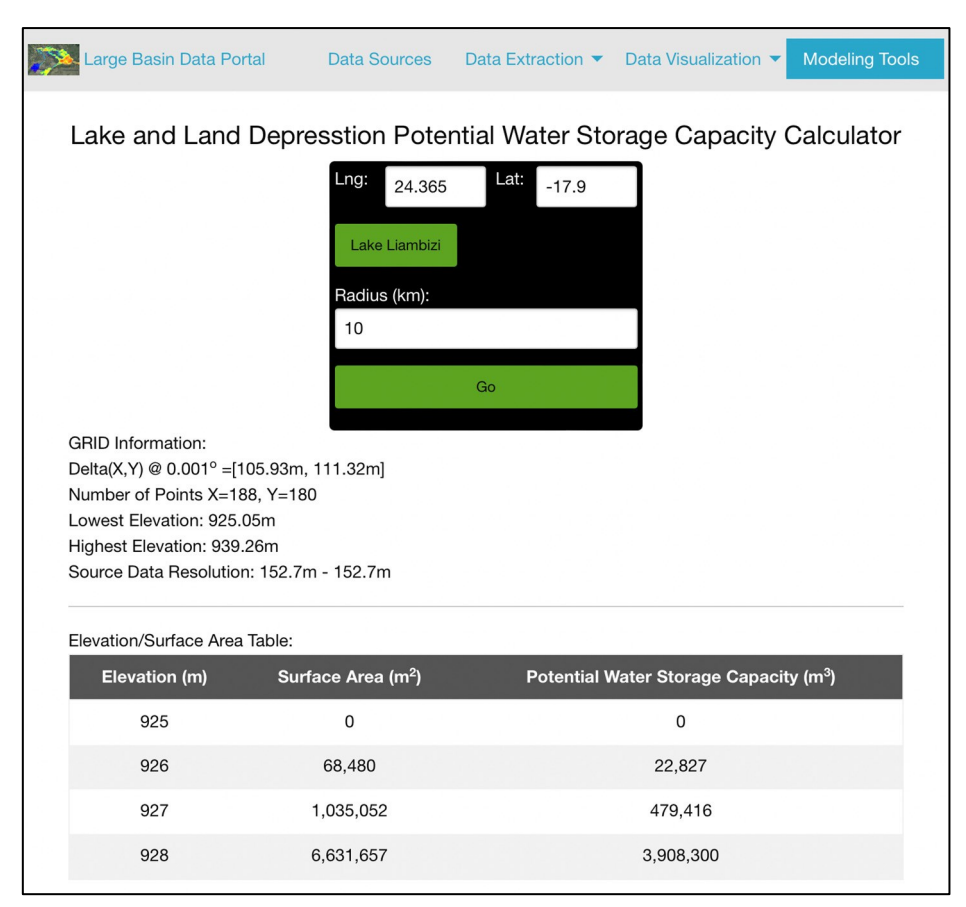


Figure 11. Screenshot of the lake storage calculator and a sample output for Lake Liambezi at the border of Botswana/Namibia showing the calculated lake water surface area and potential storage capacity when water levels increase from 925 m to 928 m above sea level. Data are derived from the Google Maps Elevation dataset.

2.5.2. UTM Coordinates Convertor

The Longitude/Latitude spherical geographical coordinate system is not ideal for modeling. In many cases, an alternate geographical coordinate system with flattened rectangular grid is used, such as the UTM system. This basic coordinates converter (Figure 12) allows the user to convert point coordinates between the two systems using the calculations described in [52].

Hydrology **2023**, 10, 87 14 of 22

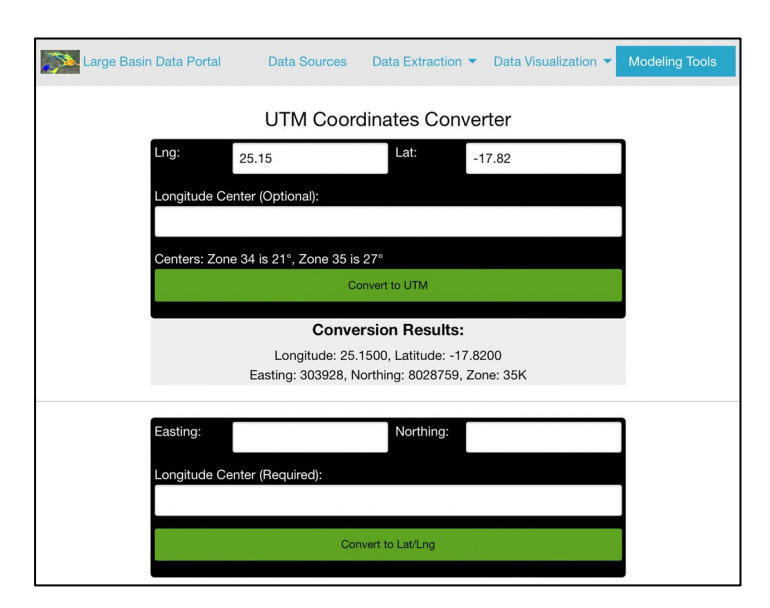


Figure 12. Screenshot of UTM coordinates conversion tool providing the ability to convert geographical coordinates between the UTM and Latitude/Longitude coordinate systems. The screenshot shows the conversion results for a sample location: Kasane, Botswana (25.15 E, 17.82 S).

2.6. Large Basin Data Portal—Database of Data Sources for Modeling

The tools that were described here use specific datasets for extraction and visualization. Other datasets are also available, and the Large Basin Data Portal includes a list of additional databases of globally available datasets with their temporal/spatial resolution and time period/spatial coverage for easy reference by users (Table A1). This resource list will be updated as new datasets are identified or become available, with key datasets added for user access within the Large Basin Data Portal.

3. Results—Case Study: The Upper Zambezi River Basin Region

Within the larger Zambezi River Basin, we focus on the Upper Zambezi River Basin region spanning Zambia, Angola, Namibia, and Botswana (Figure 13) covering an approximate area of 514 km² [53]. Local datasets for this large region are largely unavailable. Using the Large Basin Data Portal, we extracted various climatic, topographic, and soil data to create the inputs for a hydrodynamic model of the region. The hydrodynamic model was built using MIKE-SHE modeling software [39]. Data from 2009 to 2019 were extracted for the region (930 km 914 km) with a resolution of 500 m, resulting in more than 3.4 million grid cells.

Data and tools from the Large Basin Data Portal were used to create maps for the Upper Zambezi River Basin area (Figures 14-18). The elevation data extraction tool was used to extract the elevation grid for this region from the Google Maps Elevation dataset (Figure 14), and the soil type extraction tool was used to extract the soil type grid from the FAO HWSD dataset (Figure 15). Rainfall (Figure 16) and reference evapotranspiration (Figure 17) inputs were derived from the ESRL CPC Global precipitation and temperature datasets. These datasets have a resolution of 0.5, which is equivalent to approximately 55 km in the study area. Since the requested rainfall grid has a resolution of 500 m (much higher resolution than the available data), the tool clusters the 3.4 million grid cells into approximately 300 cell groups and provides a daily precipitation profile for each cell group for the requested period. The reference evapotranspiration grid was calculated from the temperature datasets and was dependent on the latitude of the grid cell, resulting in variance even between cells using the same temperature profiles. The grid cells were clustered into approximately 600 cell groups and a daily reference evapotranspiration profile was created for each cell group for the requested period. The LAI was extracted from the MODIS MOD15A2H dataset, which had a resolution of 500 m. The cells were

Hydrology **2023**, 10, 87 15 of 22

also clustered into approximately 600 cell groups based on their LAT profile for the time period (Figure 18).



Figure 13. Map of the Upper Zambezi River Basin region in Africa showing the main river branches of the basin in blue.

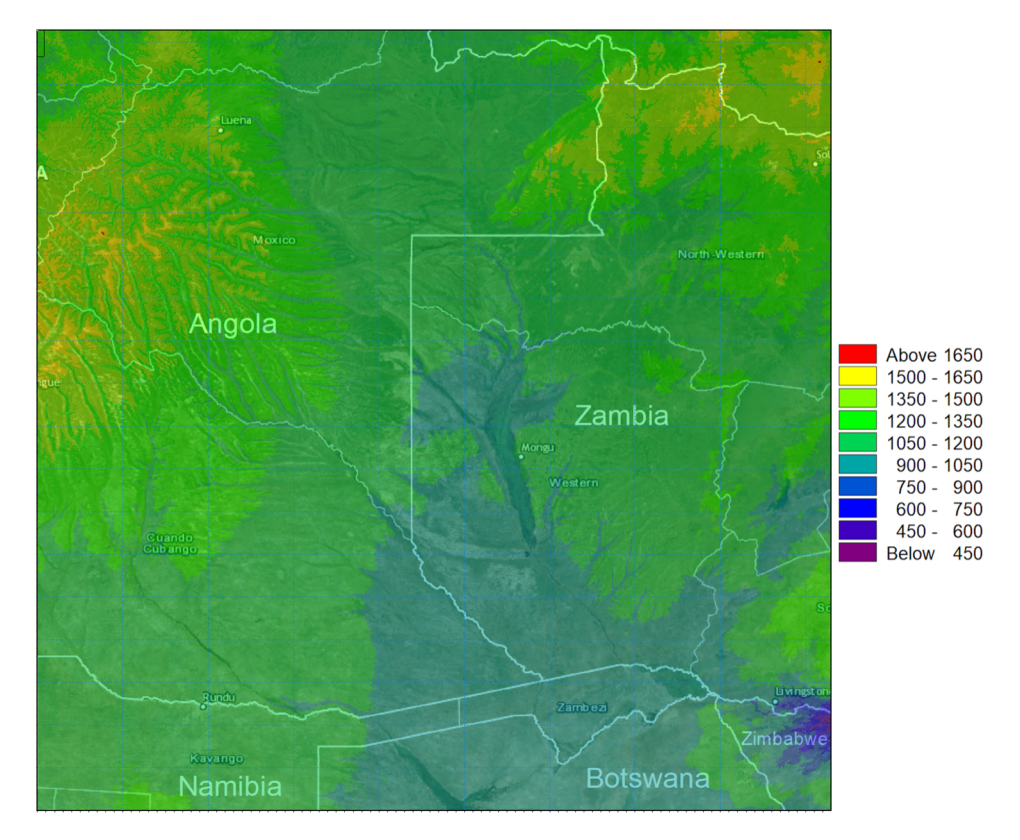


Figure 14. Screenshot of the MIKE-SHE topology grid input of the Upper Zambezi River Basin showing elevations (meters above sea level) based on data extracted using the Large Basin Data Portal tools from the Google Maps Elevation dataset.

Hydrology **2023**, 10, 87

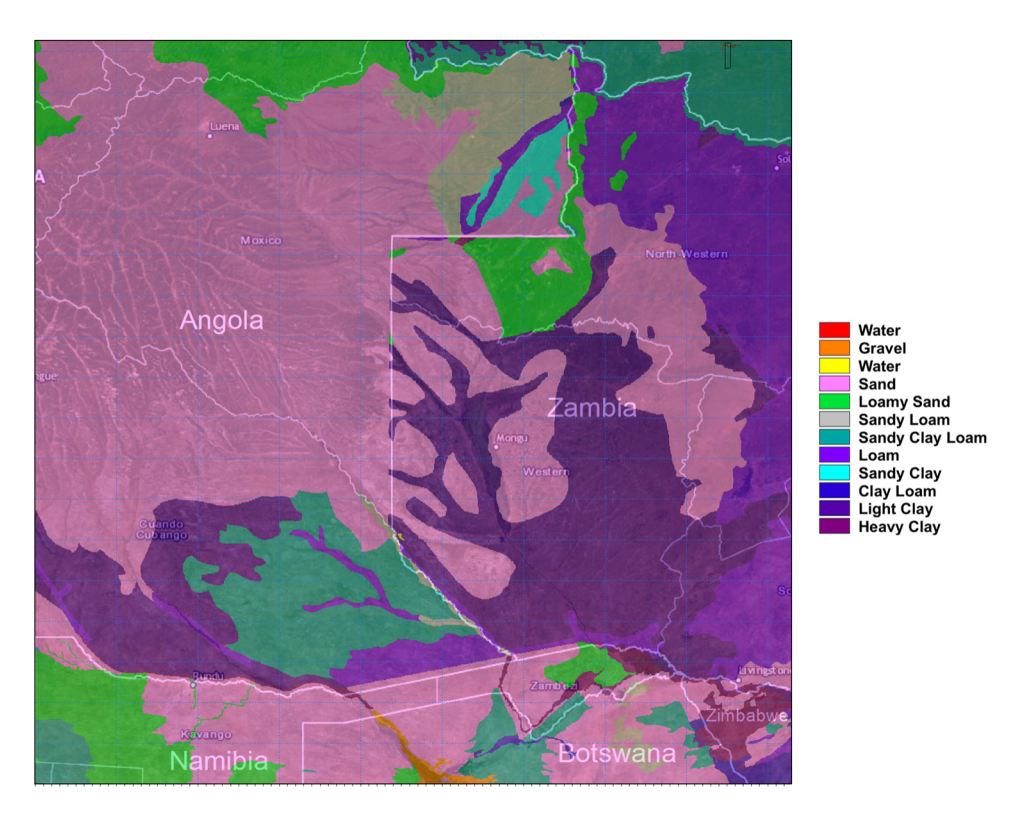


Figure 15. Screenshot of the MIKE SHE soil type input grid of the Upper Zambezi River Basin extracted using the Large Basin Data Portal tools from the FAO HWSD dataset.

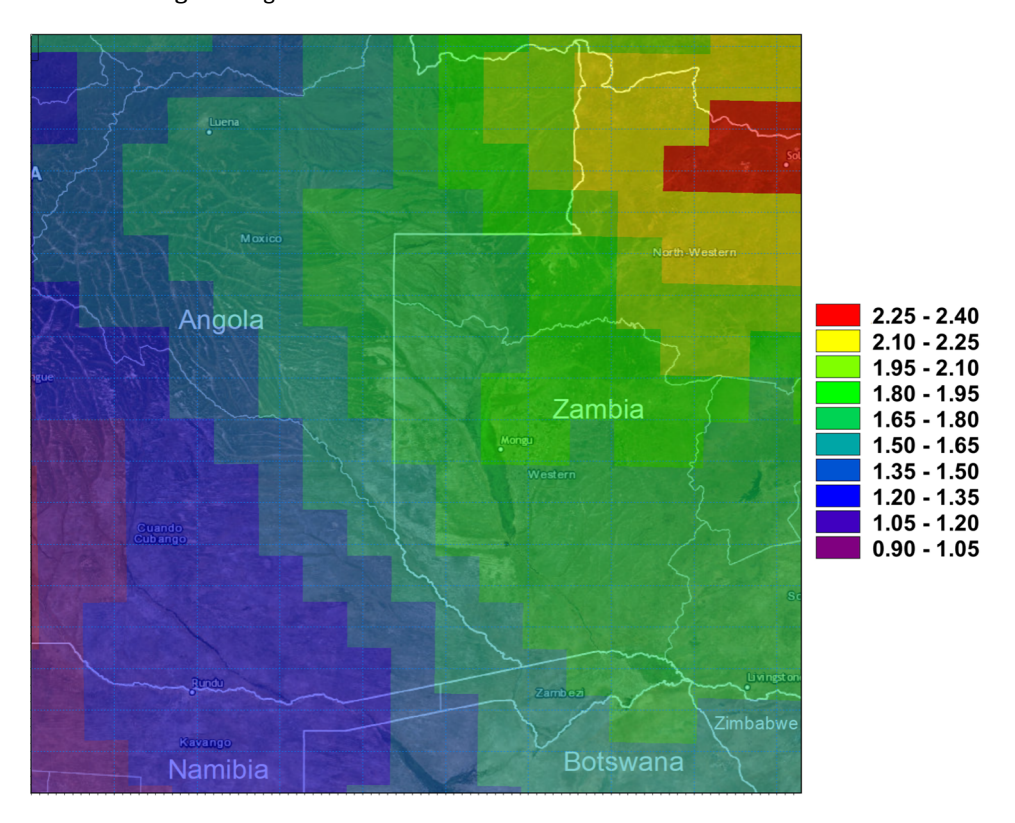


Figure 16. Screenshot of the MIKE-SHE average daily rainfall (mm/day) input grid for the Upper Zambezi River Basin extracted using the Large Basin Data Portal tools from the Earth Science Research Laboratory (ESRL) datasets for the years 2009–2019.

Hydrology **2023**, 10, 87 17 of 22

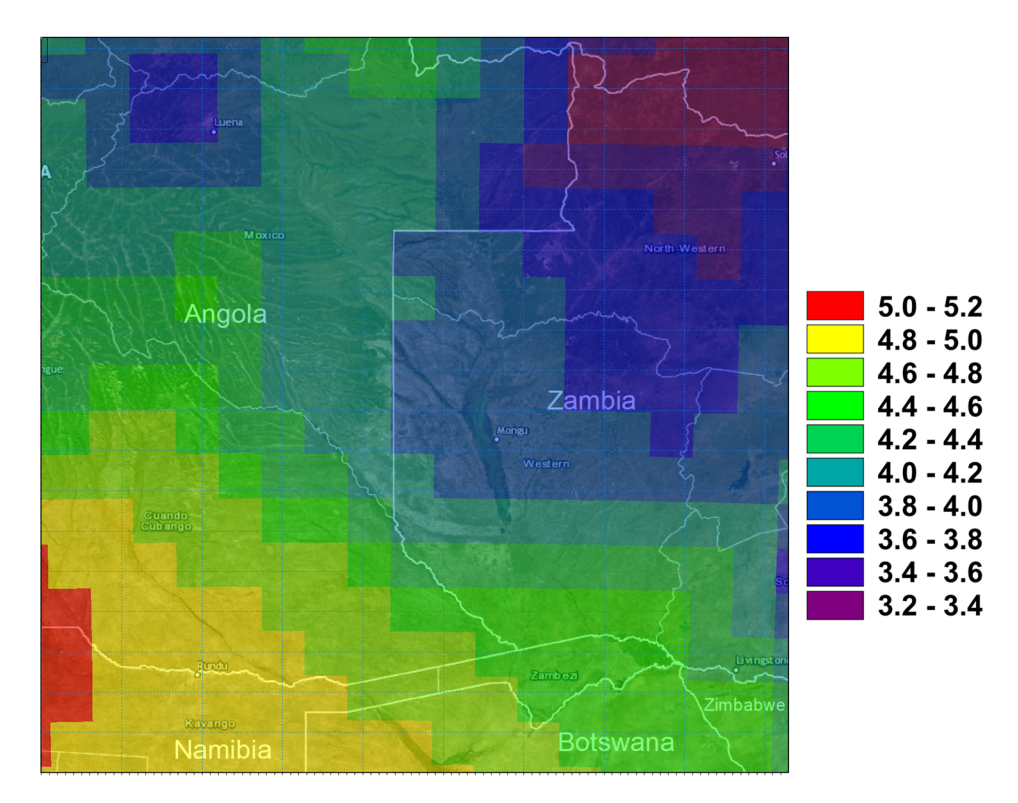


Figure 17. Screenshot of the MIKE-SHE average reference evapotranspiration (ET₀ (mm/day) input grid for the Upper Zambezi River Basin extracted using the Large Basin Data Portal based on climatic data from the Earth Science Research Laboratory (ESRL) datasets for the years 2009–2019.

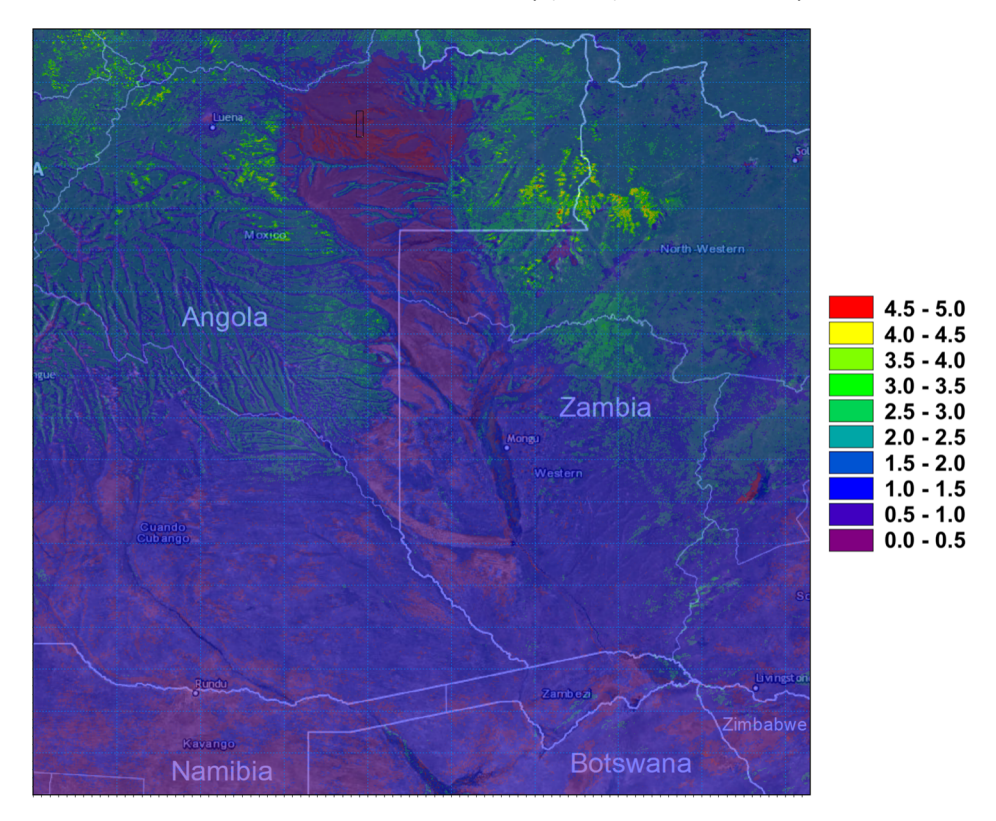


Figure 18. Screenshot of the MIKE-SHE Leaf Area Index (LAI) intensity input grid for the Upper Zambezi River Basin extracted using the Large Basin Data Portal from the MODIS datasets based on average LAI for the years 2009–2019.

Hydrology **2023**, 10, 87 18 of 22

4. Discussion

Many modelers spend a considerable amount of their time identifying, collecting, remapping, and reformatting input data for use in hydrological models. In many cases, such data are not available or not databased particularly in less developed countries. In these cases, modeling must rely on global datasets that estimate such data from satellite imaging and remote sensing resources. Many sources exist, and include NASA's MODIS terra instrument measurements, the NOAA (National Oceanic and Atmospheric Administration) ESRL data, the European Centre for Medium-Range Weather Forecasts, and FAO soil and evapotranspiration datasets, among others.

The Large Basin Data Portal developed here allows users to reduce the time and resources required to develop hydrological models and other associated applications where remote sensed data are required. The portal simplifies the process of retrieving, remapping, formatting and in some cases visualizing these data.

The portal tools developed here were successfully used to identify and extract the correct data and create the climatic and geographical inputs for a model of the Upper Zambezi River Basin region (Figures 14–18). The basin is extremely large (Figure 13), and data are limited. Modeling this region would not be possible without the utilization of remote sensing resources such as those extracted from the data portal. Indeed, it was the time required to identify these data resources that prompted the development of the Large Basin Data Portal.

With this portal, the process of generating several of the input data required to model any basin of any size, such as the Zambezi River Basin region, has now been simplified to a few clicks for many data types. The steps used to generate the input data for the Upper Zambezi River Basin model can be repeated by just modifying the required grid coordinates. The modeler can easily produce topology, rainfall, reference evapotranspiration, soil type, LAI, and land cover data for another basin.

The Large Basin Data Portal can be further improved by enhancing some of its functionalities, such as: (1) Adding the ability to select other data sources for each tool instead of a single preselected data source; (2) Adding tools to extract other types of climatic data; (3) Continually adding and updating the database of available global datasets listed in the portal; (4) Adding more output formats that may be needed for the various modeling platforms as they are updated or introduced into the market.

The use of the tools is not limited to modeling efforts. For example, the Flood Mapper can be used to explain flood hazards, assess risk, and develop contingency plans [54,55]. The extraction of elevation grids has a wide range of uses, including urban design and building dams, reservoirs, and hydraulic structures on rivers [56,57], and soil maps can be used to plan farm constructions and carry out agricultural planning [58,59].

5. Conclusions

Global datasets and modeling support tools simplify the process of building hydrodynamic models for large river basins and flood plains. The use of global datasets as inputs to large river basin models has been shown to produce results that closely correlate with actual measured river flow data [60,61]. The Large Basin Data Portal simplifies and speeds up the process of identifying data and building models, allowing modelers to direct the focus of effort on the critical steps of model parameter establishment and results analysis. Improving data access not only increases the capacity of users to contribute to such efforts, but advances our ability to harness the power of hydrological modeling to address the complex challenges that face the management of large basins across the globe.

Supplementary Materials: The following supporting information can be downloaded at: https://www.mdpi.com/article/10.3390/hydrology10040087/s1, Video S1: Large Basin Data Portal demonstration video for the data extraction tools, Video S2: Large Basin Data Portal demonstration video for the data visualization tools.

Hydrology **2023**, 10, 87 19 of 22

Author Contributions: Conceptualization, R.K.A.-S., K.A.A. and A.G.; methodology, R.K.A.-S. and K.A.A.; software development, R.K.A.-S.; validation, R.K.A.-S., K.A.A. and A.G.; formal analysis, R.K.A.-S.; investigation, R.K.A.-S.; resources, K.A.A. and A.G.; data curation, R.K.A.-S.; writing—original draft preparation, R.K.A.-S.; writing—review and editing, K.A.A.; visualization, R.K.A.-S.; supervision, K.A.A. and A.G.; project administration, K.A.A. and A.G.; funding acquisition, K.A.A. All authors have read and agreed to the published version of the manuscript.

Funding: Support for this work was partially provided by the National Science Foundation, Dynamics of Coupled Natural and Human Systems (Award #1518486, KAA), CNH2: Dynamics of Integrated Socio-Environmental Systems (Award #2009717 KAA), and Expeditions in Computing (Award #1918770 KAA).

Data Availability Statement: All data and tools presented and used in this research can be accessed from the Large Basin Data Portal link at http://caracal.info/ as of 1 April 2023.

Conflicts of Interest: The authors declare no conflict of interest.

Appendix A

Table A1. List of data sources currently databased in the Large Basin Data Portal as of 30 March 2023. The list shows the temporal and spatial resolution of the datasets, along with time period and spatial coverage.

Category	Data Type	Source and Dataset	Temporal Resolution	Time Period	Spatial Resolution	Spatial Coverage
Climate	Evaporation	European Centre for Medium-Range Weather Forecasts (ERA)	6 h	1979–Present	80 km	Worldwide
Climate	Evaporation/Transp	Global Land Evaporation Amsterdam Model (GLEAM)	Daily	1980–Present	0.25	Worldwide
Climate	Evapotranspiration	MODIS (MOD16A2)	8-Day	2001–Present	500 m	Worldwide
Climate	Precipitation	Nicholson African Monthly Rainfall Database	Monthly	1901–1984	Scattered Weather Monitoring Stations	Africa
Climate	Precipitation	WorldClim	Monthly	1970-2000	30 arc s	Worldwide
Climate	Precipitation	ESRL	Daily ¹	1979-Present (1)	0.5 ¹	Worldwide
Climate	Precipitation	National Centers for Environmental Information	Hourly/Daily	Varies by location	Scattered Weather Monitoring Stations	Worldwide
Climate	Precipitation	European Centre for Medium-Range Weather Forecasts (ERA)	6 h	1979–Present	0.4	Worldwide
Climate	Precipitation	NASA Global Precipitation Measurement	30 min ¹	2000–Present (1)	0.1 1	Worldwide
Climate	Solar Radiation	WorldClim	Monthly	1970–2000	30 arc s	Worldwide
Climate	Temperature	European Centre for Medium-Range Weather Forecasts ERA	6 h	1979–Present	0.4	Worldwide
Climate	Temperature	National Centers for Environmental Information	Hourly/Daily	Varies by location	Scattered Weather Monitoring Stations	Worldwide
Climate	Temperature (Land Surface)	MODIS (MOD11A2)	8-Day	2000–Present	1 km	Worldwide

Hydrology **2023**, 10, 87 20 of 22

Ta	h	1~	Λ	1	_	^ '	a +	
14	U		А	1.		()I		

Category	Data Type	Source and Dataset	Temporal Resolution	Time Period	Spatial Resolution	Spatial Coverage
Climate	Temperature Min/Max	ESRL	Daily ¹	1979–Present ¹	0.5 1	Worldwide
Climate	Temperature Min/Max	WorldClim	Monthly	1970–2000	30 arc s	Worldwide
Climate	Water Vapor Pressure	WorldClim	Monthly	1970–2000	30 arc s	Worldwide
Climate	Wind Speed	European Centre for Medium-Range Weather Forecasts (ERA)	6 h	1979–Present	0.4	Worldwide
Climate	Wind Speed	WorldClim	Monthly	1970–2000	30 arc s	Worldwide
Land Cover	LAI	MODIS (MOD15A2H)	8-Day	2002–Present	500 m	Worldwide
Land Cover	Land Cover	FAO HWSD	N/A	N/A	30 arc s	Worldwide
Land Cover	Land Cover Type	MODIS (MCD12Q1)	Yearly	2001–Present	500 m	Worldwide
Land Cover	Vegetation Indices	MODIS (MOD13Q1)	16-Day	2000–Present	250 m	Worldwide
Soil	Soil Type	FAO HWSD	N/A	N/A	30 arc s	Worldwide
Surface Reflectance	Surface Reflectance	MODIS (MOD09A1)	8-Day	2002–Present	500 m	Worldwide
Topography	Elevation	Google Maps Elevation	N/A	N/A	3 arc s	Worldwide
Topography	Elevation	NASA Shuttle Radar Topographic Mission	N/A	N/A	3 arc s	Worldwide
Topography	Elevation	FAO HWSD	N/A	N/A	30 arc s	Worldwide

¹ Data resolution and availability may vary by subproduct.

References

- 1. Cook, S.E.; Fisher, M.J.; Andersson, M.S.; Rubiano, J.; Giordano, M. Water, food and livelihoods in river basins. Water Int. **2009**, 34, 13–29. [CrossRef]
- 2. Loomis, J.; Kent, P.; Strange, L.; Fausch, K.; Covich, A. Measuring the total economic value of restoring ecosystem services in an impaired river basin: Results from a contingent valuation survey. Ecol. Econ. **2000**, 33, 103–117. [CrossRef]
- 3. Yang, J.; Xie, B.; Zhang, D.; Tao, W. Climate and land use change impacts on water yield ecosystem service in the Yellow River Basin, China. Environ. Earth Sci. **2021**, 80, 72. [CrossRef]
- 4. Rimal, B.; Sharma, R.; Kunwar, R.; Keshtkar, H.; Stork, N.E.; Rijal, S.; Rahman, S.A.; Baral, H. Effects of land use and land cover change on ecosystem services in the Koshi River Basin, Eastern Nepal. Ecosyst. Serv. **2019**, 38, 100963. [CrossRef]
- 5. Jain, C.K.; Singh, S. Impact of climate change on the hydrological dynamics of River Ganga, India. J. Water Clim. Chang. **2018**, 11, 274–290. [CrossRef]
- 6. Rocco, M.; Byron, O. Chapter Four—Hydrodynamic Modeling and Its Application in AUC. In Methods in Enzymology; Cole, J.L., Ed.; Academic Press: Cambridge, MA, USA, 2015; Volume 562, pp. 81–108.
- 7. Yamamoto, K.; Sayama, T.; Apip. Impact of climate change on flood inundation in a tropical river basin in Indonesia. Prog. Earth Planet. Sci. **2021**, 8, 5. [CrossRef]
- 8. Lim, T.; Spokas, K.; Feyereisen, G.; Novak, J. Predicting the impact of biochar additions on soil hydraulic properties. Chemosphere **2016**, 142, 136–144. [CrossRef]
- 9. Garg, K.K.; Karlberg, L.; Barron, J.; Wani, S.P.; Rockstrom, J. Assessing impacts of agricultural water interventions in the Kothapally watershed, Southern India. Hydrol. Process. **2012**, 26, 387–404. [CrossRef]
- 10. Taylor, J.; Lai, K.M.; Davies, M.; Clifton, D.; Ridley, I.; Biddulph, P. Flood management: Prediction of microbial contamination in large-scale floods in urban environments. Environ. Int. **2011**, 37, 1019–1029. [CrossRef]
- 11. Alexander, K.A.; Heaney, A.K.; Shaman, J. Hydrometeorology and flood pulse dynamics drive diarrheal disease outbreaks and increase vulnerability to climate change in surface-water-dependent populations: A retrospective analysis. PLoS Med. 2018, 15, e1002688. [CrossRef]
- 12. Hussainzada, W.; Lee, H.S. Hydrological Modelling for Water Resource Management in a Semi-Arid Mountainous Region Using the Soil and Water Assessment Tool: A Case Study in Northern Afghanistan. Hydrology **2021**, 8, 16. [CrossRef]
- 13. Bharati, L.; Rodgers, C.; Erdenberger, T.; Plotnikova, M.; Shumilov, S.; Vlek, P.; Martin, N. Integration of economic and hydrologic models: Exploring conjunctive irrigation water use strategies in the Volta Basin. Agric. Water Manag. 2008, 95, 925–936. [CrossRef]
- 14. Lund, J.R.; Palmer, R.N. Water Resource System M odeling for Conflict Resolution. Water Resour. Update 1997, 3, 70–82.
- 15. Nishat, B.; Rahman, S.M.M. Water Resources Modeling of the Ganges-Brahmaputra-Meghna River Basins Using Satellite Remote Sensing Data1. JAWRA J. Am. Water Resour. Assoc. **2009**, 45, 1313–1327. [CrossRef]

Hydrology **2023**, 10, 87 21 of 22

16. Dile, Y.T.; Srinivasan, R. Evaluation of CFSR climate data for hydrologic prediction in data-scarce watersheds: An application in the Blue Nile River Basin. JAWRA J. Am. Water Resour. Assoc. **2014**, 50, 1226–1241. [CrossRef]

- 17. de Paiva, R.C.D.; Buarque, D.C.; Collischonn, W.; Bonnet, M.-P.; Frappart, F.; Calmant, S.; Bulhões Mendes, C.A. Large-scale hydrologic and hydrodynamic modeling of the Amazon River basin. Water Resour. Res. **2013**, 49, 1226–1243. [CrossRef]
- 18. Pricope, N.G. Variable-source flood pulsing in a semi-arid transboundary watershed: The Chobe River, Botswana and Namibia. Environ. Monit Assess **2013**, 185, 1883–1906. [CrossRef]
- 19. Burke, J.J. Modeling Surface Inundation and Flood Risk in a Flood-Pulsed Savannah: Chobe River, Botswana and Namibia; University of North Carolina Wilmington: Wilmington, NC, USA, 2015.
- 20. Burke, J.J.; Pricope, N.G.; Blum, J. Thermal Imagery-Derived Surface Inundation Modeling to Assess Flood Risk in a Flood-Pulsed Savannah Watershed in Botswana and Namibia. Remote Sens. **2016**, 8, 676. [CrossRef]
- Long, S.; Fatoyinbo, T.E.; Policelli, F. Flood extent mapping for Namibia using change detection and thresholding with SAR. Environ. Res. Lett. 2014, 9, 035002. [CrossRef]
- 22. McCarthy, J.M.; Gumbricht, T.; McCarthy, T.; Frost, P.; Wessels, K.; Seidel, F. Flooding Patterns of the Okavango Wetland in Botswana between 1972 and 2000. AMBIO J. Hum. Environ. **2003**, 32, 453–457. [CrossRef]
- 23. Braget, M.P.; Goodin, D.G.; Wang, J.; Hutchinson, J.M.S.; Alexander, K. Flooded area classification using pooled training samples: An example from the Chobe River Basin, Botswana. J. Appl. Remote Sens. **2018**, 12, 026033. [CrossRef]
- 24. Geleta, H.I. Watershed Sediment Yield Modeling for Data Scarce Areas; Universitat Stuttgart: Stuttgart, Germany, 2011.
- 25. Tegegne, G.; Park, D.K.; Kim, Y.-O. Comparison of hydrological models for the assessment of water resources in a data-scarce region, the Upper Blue Nile River Basin. J. Hydrol. Reg. Stud. **2017**, 14, 49–66. [CrossRef]
- Chen, L.; Sun, C.; Wang, G.; Xie, H.; Shen, Z. Event-based nonpoint source pollution prediction in a scarce data catchment.
 J. Hydrol. 2017, 552, 13–27. [CrossRef]
- 27. Johnston, R.; Smakhtin, V. Hydrological Modeling of Large river Basins: How Much is Enough? Water Resour. Manag. **2014**, 28, 2695–2730. [CrossRef]
- 28. Ireson, A.; Makropoulos, C.; Maksimovic, C. Water resources modelling under data scarcity: Coupling MIKE BASIN and ASM groundwater model. Water Resour. Manag. 2006, 20, 567–590. [CrossRef]
- 29. Swain, S.S.; Mishra, A.; Sahoo, B.; Chatterjee, C. Water scarcity-risk assessment in data-scarce river basins under decadal climate change using a hydrological modelling approach. J. Hydrol. **2020**, 590, 125260. [CrossRef]
- 30. Zambezi River Authority: Geography of the Zambezi River. Available online: http://www.zambezira.org/hydrology/geography (accessed on 15 February 2023).
- 31. Schultz, G.A. Hydrological modeling based on remote sensing information. Adv. Space Res. 1993, 13, 149–166. [CrossRef]
- 32. Alexander, K.A.; Blackburn, J.K. Overcoming barriers in evaluating outbreaks of diarrheal disease in resource poor settings: Assessment of recurrent outbreaks in Chobe District, Botswana. BMC Public Health **2013**, 13, 775. [CrossRef]
- 33. Moore, A.E.; Cotterill, F.P.; Main, M.P.; Williams, H.B. The zambezi river. In Large Rivers: Geomorphology and Management; John Wiley & Sons: Hoboken, NJ, USA, 2007; pp. 311–332.
- 34. Beyer, M.; Wallner, M.; Bahlmann, L.; Thiemig, V.; Dietrich, J.; Billib, M. Rainfall characteristics and their implications for rain-fed agriculture: A case study in the Upper Zambezi River Basin. Hydrol. Sci. J. **2016**, 61, 321–343. [CrossRef]
- 35. PHP: PHP Hypertext Processor. Available online: https://www.php.net/docs.php (accessed on 15 February 2023).
- 36. The GNU C Reference Manual. Available online: https://www.gnu.org/software/gnu-c-manual/gnu-c-manual.html (accessed on 29 March 2023).
- 37. Slater, J.A.; Malys, S. WGS 84—Past, Present and Future; SpringerLink: Berlin, Germany, 1998; pp. 1–7.
- 38. Lu, G.Y.; Wong, D.W. An adaptive inverse-distance weighting spatial interpolation technique. Comput. Geosci. **2008**, 34, 1044–1055. [CrossRef]
- 39. DHI. MIKE-SHE (Version 2022). Windows. DHI. 2022. Available online: https://www.mikepoweredbydhi.com/download/mike-2022 (accessed on 8 March 2023).
- 40. Lloyd, S. Least squares quantization in PCM. IEEE Trans. Inf. Theory 1982, 28, 129–137. [CrossRef]
- 41. NASA: Flooding on the Zambezi River. Available online: https://earthobservatory.nasa.gov/images/83667/flooding-on-the-zambezi-river (accessed on 15 February 2023).
- 42. Google. Google Maps Platforms. Available online: http://mapsplatform.google.com (accessed on 20 February 2023).
- 43. FAO; IIASA; ISRIC; ISSCAS; JRC. Harmonized World Soil Database (Version 1.2). 2012. Available online: https://www.fao.org/soils-portal/data-hub/soil-maps-and-databases/harmonized-world-soil-database-v12/en/ (accessed on 20 February 2023).
- 44. PSL, N.O.E. CPC US Unified Precipitation da. 2022. Available online: https://psl.noaa.gov/data/gridded/data.cpc.globalprecip. html (accessed on 20 February 2023).
- 45. Myneni, R.; Knyazikhin, Y.; Park, T. MYD15A2H MODIS/Aqua Leaf Area Index/FPAR 8-Day L4 Global 500m SIN Grid. 2015. Available online: https://lpdaac.usgs.gov/products/myd15a2hv006/ (accessed on 20 February 2023). [CrossRef]
- 46. Allan, R.; Pereira, L.; Smith, M. Crop Evapotranspiration-Guidelines for Computing Crop Water Requirements-FAO Irrigation and Drainage Paper 56; FAO: Rome, Italy, 1998; Volume 56.
- 47. Hargreaves, G.; Samani, Z. Reference Crop Evapotranspiration From Temperature. Appl. Eng. Agric. 1985, 1, 96–99. [CrossRef]
- 48. Vermote, E. MOD09A1 MODIS Surface Reflectance 8-Day L3 Global 500m SIN Grid V006. 2015. Available online: https://lpdaac.usgs.gov/products/mod09a1v006/ (accessed on 20 February 2023).

Hydrology **2023**, 10, 87 22 of 22

49. Sun, D.; Yu, Y.; Goldberg, M.D. Deriving Water Fraction and Flood Maps From MODIS Images Using a Decision Tree Approach. IEEE J. Sel. Top. Appl. Earth Obs. Remote Sens. **2011**, 4, 814–825. [CrossRef]

- 50. Friedl, M.S.-M.D. MCD12Q1 MODIS/Terra+Aqua Land Cover Type Yearly L3 Global 500m SIN Grid V006. 2019. Available online: https://lpdaac.usgs.gov/products/mcd12q1v006/ (accessed on 20 February 2023).
- 51. Taube, C.M. Instructions for winter lake mapping. In Manual of Fisheries Survey Methods II: With Periodic Updates; Schneider, J.C., Ed.; Fisheries Special Report 25; Michigan Department of Natural Resources: Ann Arbor, MI, USA, 2000; Chapter 12.
- 52. Kelly, K.M. Universal Transverse Mercator/Geographic Coordinate Transformations; Ontario Ministry of Natural Resources: Vancouver, BC, Canada, 1986.
- 53. Beilfuss, R. A Risky Climate for Southern African Hydro: Assessing hydrological risks and consequences for Zambezi River Basin Dams; International Rivers: Berkeley, CA, USA, 2012.
- 54. Seipel, S.; Lim, N.J. Color map design for visualization in flood risk assessment. Int. J. Geogr. Inf. Sci. **2017**, 31, 2286–2309. [CrossRef]
- 55. Auliagisni, W.; Wilkinson, S.; Elkharboutly, M. Using community-based flood maps to explain flood hazards in Northland, New Zealand. Prog. Disaster Sci. **2022**, 14, 100229. [CrossRef]
- 56. Moughtin, C.; Oc, T.; Tiesdell, S. Urban Design: Ornament and Decoration; Routledge: Abingdon, UK, 1999.
- 57. Khattab, M.F.; Abo, R.K.; Al-Muqdadi, S.W.; Merkel, B.J. Generate reservoir depths mapping by using digital elevation model: A case study of Mosul dam lake, Northern Iraq. Adv. Remote Sens. 2017, 6, 161–174. [CrossRef]
- 58. Holst, K.A.; Madsen, H.B. The elaboration of drainage class maps for agricultural planning in Denmark. Landsc. Urban Plan. **1986**, 13, 199–218. [CrossRef]
- 59. Vella, S. Soil survey and soil mapping in the Maltese Islands: The 2003 position. Eur. Soil Bur. Res. Rep. 2003, 9, 235-244.
- 60. Gosling, S.N.; Arnell, N.W. Simulating current global river runoff with a global hydrological model: Model revisions, validation, and sensitivity analysis. Hydrol. Process. **2011**, 25, 1129–1145. [CrossRef]
- 61. Nijssen, B.; O'Donnell, G.M.; Lettenmaier, D.P.; Lohmann, D.; Wood, E.F. Predicting the discharge of global rivers. J. Clim. **2001**, 14, 3307–3323. [CrossRef]

Disclaimer/Publisher's Note: The statements, opinions and data contained in all publications are solely those of the individual author(s) and contributor(s) and not of MDPI and/or the editor(s). MDPI and/or the editor(s) disclaim responsibility for any injury to people or property resulting from any ideas, methods, instructions or products referred to in the content.